Comparison of Tissue Homogeneity Tracer Kinetics Models on Pixel-by-Pixel DCE MRI Data in Breast Tumors

Dennis Lai Hong Cheong[1,2], Thian Chor Ng[3,4], Bo Zhang[1,5], Bingwen Zheng[1], Eugene Mun Wai Ong[4], and Soo Chin Lee[6,7]

[1]Clinical Imaging Research Center, A*STAR & National University of Singapore, Singapore, Singapore, [2]Neuroradiology Department, National Neuroscience Institute, 308433, Singapore, [3]Clinical Imaging Research Center, A*STAR & National University of Singapore, Singapore, Singapore, [4]Department of Radiology, National University of Singapore, 119074, Singapore, [5]Quantitative Image Processing Group, SBIC/A*STAR, 138671, Singapore, [6]Department of Haematology-Oncology, National University Health System, 119074, Singapore, [7]Cancer Science Institute, 117456, Singapore

Introduction

Conventional compartmental tracer kinetics (TK) models have been commonly used for analysis of DCE MRI data. Although distributed parameter (DP) models [1] (e.g. tissue homogeneity (TH) models [2]) are theoretically more realistic, it has not gained much popularity. Some groups recently suggested the importance of selecting a tracer kinetic model that is appropriate for the dataset being analyzed [3,4]. Recent advancements in the hybrid DP models [5,6] and their implementation [7] have allowed us to apply them at pixel-by-pixel level. To the best of our knowledge, comparison of TK models involving TH models on pixel-by-pixel DCE MRI data have not been reported. This work is a part of our DCE-MRI projects in both treated and untreated breasts.

Methods

MRI scans were performed with a whole-body 3T MR scanner (Magnetom Trio; Siemens, Germany) and a breast receiver coil including an additional surface coil placing on the back of patients (n=9) for direct measurements of arterial input function (AIF) from the aorta. With 3D spoiled FLASH, pre-contrast T1 maps (TR=20ms, FA= 5°,13°,20°, matrix 256×256, 16 slices, 4-mm slice thickness) and subsequent dynamic acquisition (TR=4ms, FA=15°, matrix 128×128 interpolated to 256×256, and temporal resolution 2.4s per frame for 200 frames) [8]. On the seventh dynamic time-point, 0.1 mmol/kg of body weight dosage of 0.5 M Gadolinium-based contrast agent (Magnevist, Bayer, Germany) was administered through a power injector at a rate of 3 ml/s. Tumor ROIs were drawn by a radiologist. Pixel-by-pixel contrast concentration time curves extracted from the tumor region on all slices were analyzed using a two-compartment axially DP (axDP2) model [6], adiabatic approximation to TH model (AATH) [5], Tofts model (TM) and the extended Tofts model (ETM) [9,10]. We analyzed 2973 concentration curves extracted from a representative tumor.

Fig. 1 Fitting errors of TM, ETM and AATH models plotted against axDP2 model.

Results

AATH and axDP2 models achieved almost identical fitting errors (0.228±0.152 and 0.231±0.152 mM, respectively) (Fig. 1). TM and ETM models fitting errors (0.511±0.551 and 0.281±0.213 mM, respectively) were generally larger than the two DP models, with TM model consistently worse than ETM model (Fig. 1).

Fig. 2(a) shows three typical concentration time curves and the fitted curves by the four TK models and Fig. 2(b-d) show their impulse residue functions (IRF). ETM IRF includes a Dirac delta function that is not shown. In TM and ETM IRFs, the peak on the left is the transfer constant (K^{trans}). For AATH and axDP2 IRFs, the start of the decaying curve is the product of first pass extraction ratio (E) and perfusion (F), EF. The starting time of IRF (Fig. 2b-d) is the lag time of contrast material arrival at the tumor from that at where AIF is measured.

Generally, K^{trans} from TM > K^{trans} from ETM > EF and permeability surface area product (PS) from both axDP2 and AATH models (Fig. 2b-d, 3a, Table 1). Similar trend is seen in the comparison of fractional extravascular extracellular volume, v_e (Fig. 3b). Table 1 also list values (median, mean±SD) of fractional intravascular space (v_p) and lag time.
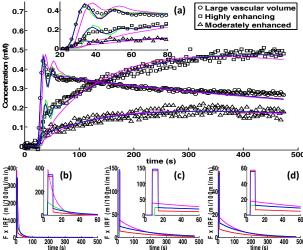

Fig. 2 Three typical concentration time curves from data (a, symbols) and their corresponding curve fittings (a, lines) and IRFs (b-d) of axDP2 (blue lines), ATH (red lines), ETM (green lines) and TM (magenta lines) models are shown. Insets in figures show the first 60 s.

Table 1. Parameter values (median, mean±SD) from the four TK models.

	TM	ETM	AATH	axDP2
K^{trans} or EF (ml/100ml/min)	41.7, 85.1±120	19.2, 29.0±31.2	8.91, 12.8±12.9	9.28, 14.2±13.1
v_e (%)	54.3, 57.5±26.6	44.9, 49.3±25.3	24.0, 27.3±16.4	22.0, 24.5±13.9
v_p (%)	N.A.	13.7, 1.9±11.4	9.84, 11.8±8.69	9.63, 11.5±8.56
F (ml/100ml/min)	N.A.	N.A.	99.1, 123±91.3	102, 128±94.3
PS (ml/100ml/min)	N.A.	N.A.	9.87, 14.6±15.5	10.2, 15.0±15.8
Lag time (s)	fixed to AATH's	8.96, 9.85±3.92	6.95, 7.78±3.80	7.18, 7.94±3.78

Discussion

AATH approximated axDP2 model very closely (Fig. 1). TM and ETM models have larger fit errors but were still able to give appropriate fittings (Fig. 2a). However both models were found to be inappropriate for voxels with significant vascular volume (Fig. 2(a,b)). Although ETM model included a vascular compartment using a scaled down version of the AIF, which has narrower peak as our AIF was from the aorta. This might have led to larger estimation of the lag time (Table 1, Fig. 2b,c). TM and ETM K^{trans} are larger than EF in DP models (Fig. 3a) could be due to K^{trans} is defined as the initial value of their IRFs (Fig. 2b-d). In pixel-by-pixel analysis of DCE MRI data in tumors, our preliminary data suggests that DP models are better than compartmental models by having better fittings (Fig. 1 and 2) and more stable parameter values (Fig. 3, Table 1).
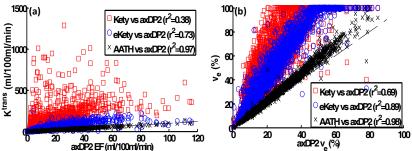

Fig. 3 Scattered plots of K^{trans} of TM (red squares) and ETM (blue circles), EF of AATH (black crosses) against EF of DP models (a) and v_e (b). Dashed lines are identity lines.

References

1. Koh TS et al. J Magn Reson Imaging. 2011;doi:10.1002/jmri.22795.
2. Johnson and Wilson. Am J Physiol 1966;210:1299–1303.
3. Donaldson SB et al. Magn Reson Med 2010;63:691–700.
4. Sourbron SP and Buckley DL. Magn Reson Med 2011;66:735–745.
5. St. Lawrence KS and Lee TY. J Cereb Blood Flow Metab 1998;18:1365–1385.
6. Koh TS et al. IEEE Trans Biomed Eng 2003;50:159–167.
7. Koh TS et al. Magn Reson Med 2011;66:886–892.
8. Zheng BW et. al. ISMRM 2011;1676.
9. Tofts PS. J Magn Reson Imaging 1997;7:91–101.
10. Tofts PS et al. J Magn Reson Imaging 1999;10:223–232.